Developmental Cell
Article

Apelin and Its Receptor Control Heart Field Formation during Zebrafish Gastrulation

Xin-Xin I. Zeng,[1,2] Thomas P. Wilm,[1,2] Diane S. Sepich,[1] and Lilianna Solnica-Krezel[1,*]
[1] Vanderbilt University, Department of Biological Sciences, VU Station B 35-1634, Nashville, TN 37235, USA
[2] These authors contributed equally to this work.
*Correspondence: lilianna.solnica-krezel@vanderbilt.edu
DOI 10.1016/j.devcel.2007.01.011

SUMMARY

The vertebrate heart arises during gastrulation as cardiac precursors converge from the lateral plate mesoderm territories toward the embryonic midline and extend rostrally to form bilateral heart fields. G protein-coupled receptors (GPCRs) mediate functions of the nervous and immune systems; however, their roles in gastrulation remain largely unexplored. Here, we show that the zebrafish homologs of the Agtrl1b receptor and its ligand, Apelin, implicated in physiology and angiogenesis, control heart field formation. Zebrafish gastrulae express *agtrl1b* in the lateral plate mesoderm, while *apelin* expression is confined to the midline. Reduced or excess Agtrl1b or Apelin function caused deficiency of cardiac precursors and, subsequently, the heart. In Apelin-deficient gastrulae, the cardiac precursors converged inefficiently to the heart fields and showed ectopic distribution, whereas cardiac precursors overexpressing Apelin exhibited abnormal morphology and rostral migration. Our results implicate GPCR signaling in movements of discrete cell populations that establish organ rudiments during vertebrate gastrulation.

INTRODUCTION

The vertebrate body plan, germ layers, and organ rudiments are established during gastrulation via concurrent inductive and morphogenetic events. Internalization generates the three germ layers when endodermal and mesodermal precursors move beneath the prospective ectodermal layer. The process of epiboly spreads and thins the germ layers. Convergence movements narrow the germ layers mediolaterally, while extension movements elongate them anteroposteriorly. Several signaling pathways have been implicated in directing these large-scale gastrulation movements in vertebrates, including Stat3, noncanonical Wnt, and FGF signaling (Keller, 2005; Leptin, 2005; Solnica-Krezel, 2005). G protein-coupled receptors (GPCRs) have been linked to chemotaxis in *Dictyostellium discoideum* and in the mammalian immune system (Devreotes and Janetopoulos, 2003). They have prominent roles in sensory organs and the central nervous system in adults. However, their roles in vertebrate gastrulation are not understood. In fact, little is known about the developmental expression and/or function of any of the close to 400 endo-GPCRs encoded in the human genome (Vassilatis et al., 2003). Recent studies indicate that heterotrimeric G proteins, which transduce signals downstream of GPCRs to regulate cell migration, are also essential for the gastrulation movements of epiboly, convergence, and extension in zebrafish (Lin et al., 2005). However, the identity of the corresponding GPCRs remains to be determined.

Here, we implicate a chemokine, Apelin, and its receptor, Agtrl1b, in convergence and extension gastrulation movements of cardiac precursors in zebrafish. Angiotensin II receptor-like 1 (Agtrl1, also named APJ), initially identified as an "orphan" receptor, was shown to be activated by a 36 amino acid peptide from bovine stomach homogenates (Tatemoto et al., 1998). Subsequently, a 77 amino acid prepropeptide of a novel ligand, called Apelin for Agtrl1 endogenous ligand, was identified in human and bovine tissues. Peptides of varying size comprising C-terminal fragments of the Apelin prepropeptide can activate the receptor (Habata et al., 1999; Kawamata et al., 2001; Lee et al., 2000). Several studies have reported cardiovascular actions of Apelin/Agtrl1, including regulation of blood pressure in vivo (Tatemoto et al., 2001) and exertion of positive inotropic effects in the heart (Berry et al., 2004; Szokodi et al., 2002), in humans. Reports of declining Apelin/Agtrl1 levels in patients with chronic heart failure imply that this signaling system may have cardioprotective properties (Chen et al., 2003). More recently, *apelin* has been shown to be required for normal vascular development in frog embryos (Inui et al., 2006).

The heart anlage arises during gastrulation when prospective cardiac precursors, specified in the lateral plate mesoderm territories, converge toward the embryonic midline and extend rostrally to form bilateral heart fields at late gastrulation (Keegan et al., 2004). The two heart fields fuse during segmentation into a single heart tube (Auman and Yelon, 2004; Moorman and Christoffels, 2003; Yelon and Stainier, 1999). In zebrafish, lysosphingolipid signaling via the Miles apart GPCR is essential for movements and fusion of the bilateral heart primordia during segmentation (Kupperman et al., 2000). Whether

similar pathways that regulate movements of defined cell populations also operate during vertebrate gastrulation is an open question.

We provide several lines of evidence that Apelin and its Agtrl1b receptor regulate heart precursor cell movements during zebrafish gastrulation. Whereas *agtrl1b* is expressed in the lateral plate mesoderm, *apelin* expression is confined to the midline, where signals regulating convergence and extension movements are thought to reside (Solnica-Krezel, 2005). Reduction or excess Agtrl1b or Apelin expression impaired cardiac precursor and heart formation, whereas other embryonic tissues were only mildly affected. In gastrulae overexpressing or deficient in Apelin, the cardiac precursors moved inefficiently to the heart fields and exhibited abnormal morphology and protrusive activity.

To our knowledge, our work uncovers a novel role of Apelin/Agtrl1b signaling in mediating heart field formation during zebrafish gastrulation. These findings implicate GPCR signaling in cell movements that establish organ rudiments during gastrulation and suggest that vertebrate gastrulation employs pathways that govern movements of all gastrula cells or entire germ layers, as well as pathways that regulate movements of discrete cell populations.

RESULTS

Complementary Expression of the Agtrl1b Receptor and Its Ligand, Apelin, in Zebrafish Gastrulae

In our efforts to identify GPCRs regulating vertebrate gastrulation, we isolated zebrafish homologs of Angiotensin II receptor-like 1 (Agtrl1), *agtrl1b* and *agtrl1a*, and its putative ligand, Apelin (*apln*). *agtrl1a* is not described here, but its cloning and expression pattern have been recently reported (Tucker et al., 2007). Agtrl1b and Apelin have been previously identified in human, mouse, and *Xenopus laevis* (Figure S1; see the Supplemental Data available with this article online) (Devic et al., 1996, 1999; O'Dowd et al., 1993). Our analysis of the spatiotemporal *agtrl1b* and *apln* expression suggested involvement of these molecules in gastrulation and heart development. By whole-mount in situ hybridization, *agtrl1b* expression was first detected after the onset of zygotic transcription in randomly positioned cells in the blastoderm (Figure 1A). By 4.5 hr postfertilization (hpf), mesendodermal precursors at the blastoderm margin started to express *agtrl1b* (Figure 1B). At early gastrulation, marginal *agtrl1b* expression was maintained ventrolaterally, while expression in dorsal cells and in random deep cells declined (Figures 1C and 1D). During gastrulation and segmentation, *agtrl1b* expression was maintained in adaxial, intermediate, and lateral plate mesoderm (LPM), including the anterior LPM, where the heart precursors reside (Figures 1E and 1F) (Keegan et al., 2004). During late segmentation, several *agtrl1b* expression domains were detected, including those in the forming heart, as revealed by coexpression with the heart marker *cardiac myosin light chain 2* (*cmlc2*) (Figures 1G–1I). By 24 hpf, *agtrl1b* expression was detected in dorsal aorta, caudal vein, and intersomitic blood vessels (Figures 1J and 1K). Expression in blood vessels declined by 1.5 days postfertilization (dpf) and was undetectable at 2 dpf (data not shown).

Transcripts of the Agtrl1b ligand, Apelin, were first detected at midgastrulation by RT-PCR (Figure 1L). Interestingly, whole-mount in situ hybridization revealed that *apln* expression complemented that of *agtrl1b* during gastrulation: *apln* transcripts were detected exclusively in the axial mesoderm and its later derivative, the notochord (Figures 1M–1O). At late segmentation, *apln* expression was maintained posteriorly in the forming notochord (Figure 1P), and new expression was identified in the presumptive heart, coinciding with expression of its receptor (Figures 1I, 1K, and 1P). By 24 hpf, discrete *apln* expression domains appeared in the head (Figure 1Q).

Reduced and Excess Agtrl1b Impair Gastrulation and Heart Formation

To investigate the role of Apelin and its receptor during zebrafish development, we misexpressed the Agtrl1b receptor by microinjecting synthetic RNA into 1-cell-stage embryos. The earliest effects were detected at 4 hpf, when the interface between the blastoderm and the yolk cell showed strong distortions (Figures 2A and 2B). As *apelin* is not expressed until 7 hpf, and constitutive activity in a ligand-independent manner was reported for GPCRs (Smit et al., 2006), we attribute these effects to excess receptor activity. Subsequently, the progress of epiboly and other gastrulation movements was variably compromised (data not shown). Nevertheless, by the end of the gastrula period, all injected embryos manifested normal anterior-posterior (AP) axis extension, although 85% exhibited mediolateral broadening of neuroectodermal and mesodermal tissues compared to uninjected siblings (n = 265, 400 pg; Figures 2C–2F), and by 24 hpf injected embryos were of normal length or slightly shorter (data not shown). Analyses of tissue-specific markers revealed that embryonic patterning and tissue specification were not compromised by the injection of *agtrl1b* RNA, except for a small reduction in myocardial marker expression (n = 234, 400 pg; Figures 2E, 2F, 3A, and 3C; data not shown). These results suggest that the correct expression level and spatial distribution of Agtrl1b are crucial for normal gastrulation movements.

We assessed the requirement for Agtrl1b during gastrulation by using antisense morpholino oligonucleotides ($MO^{agtrl1b}$) designed to interfere with its translation (Nasevicius and Ekker, 2000). Whereas all embryos injected with synthetic RNA encoding carboxyl terminus HA-tagged Agtrl1b alone exhibited membrane-bound receptor (n = 5), Agtrl1b-HA expression was downregulated in embryos coinjected with $MO^{agtrl1b}$ (n = 10; Figures 2G and 2H), supporting the effectiveness of $MO^{agtrl1b}$ in inhibiting Agtrl1b translation. Embryos injected with 1 or 2 ng $MO^{agtrl1b}$ showed an almost normal mediolateral axis with a dose-dependent reduction of the AP axis at late gastrulation (Figures 2I and 2J and data not shown), but only minor changes in general tissue specification and patterning

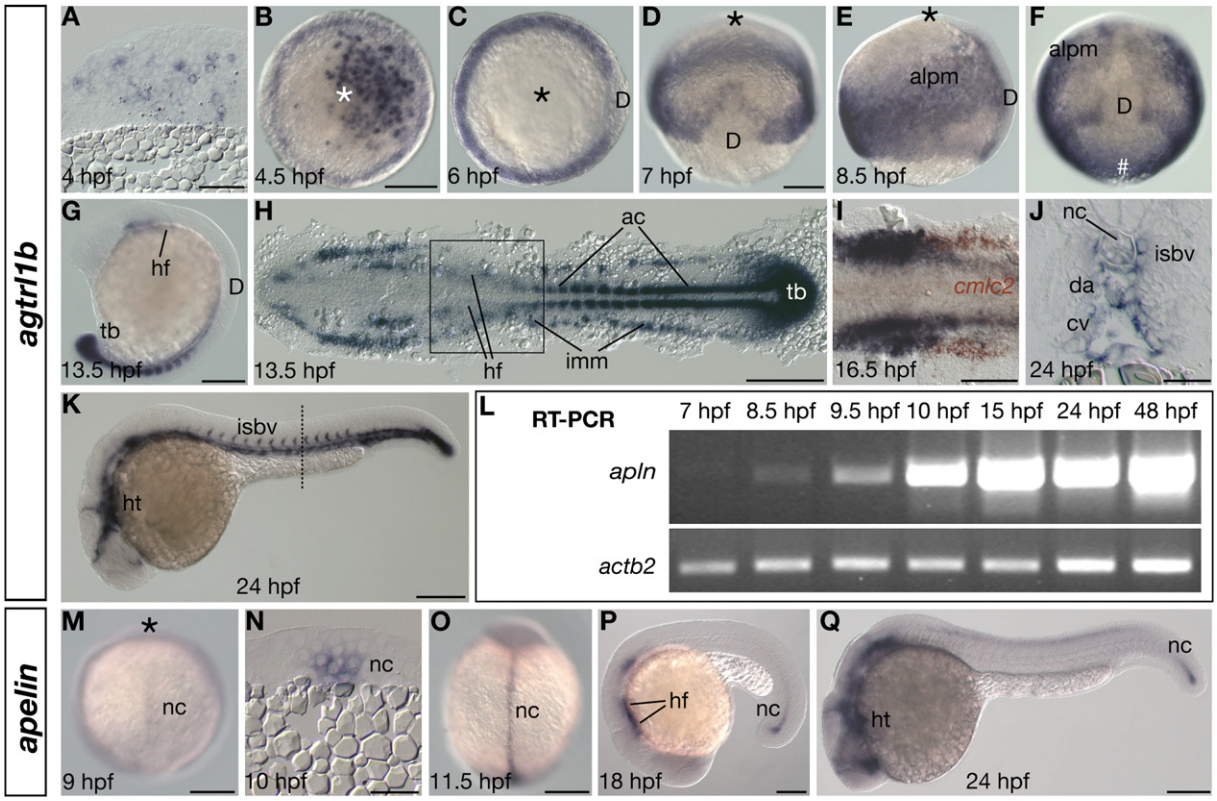

Figure 1. Spatiotemporal Expression of *agtrl1b* and *apln* during Zebrafish Embryogenesis

(A–K) *agtrl1b* expression profile. (A) *agtrl1b* expression in deep cells at 4 hpf. (B) At 4.5 hpf, *agtrl1b* expression appears at the blastoderm margin. (C) At the onset of gastrulation, *agtrl1b* expression is only maintained in the blastoderm margin. (D–F) *agtrl1b* expression during gastrulation in the anterior lateral plate mesoderm (alpm) and the posterior and adaxial mesoderm. (G and H) New *agtrl1b* expression domains in the developing brain, adaxial cells (ac), intermediate mesoderm (imm), and heart field (hf) at early segmentation stages (8 somites); tailbud (tb). (G) Lateral view. (H) Flat mount; anterior is oriented toward the left. (I) Boxed region in (H). By midsegmentation (14 somites), *agtrl1b* expression in cardiac precursors overlaps with *cmlc2* (red). (J and K) New *agtrl1b* expression in dorsal aorta (da), caudal vein (cv), and intersomitic blood vessels (isbv) at 24 hpf. (J) Cross-section through the trunk region marked by a dashed line in (K). Notochord, nc.

(L–Q) *apln* expression profile. (L) RT-PCR of *apln* transcript at 7–48 hpf; *β-actin* (*actb2*) was used as a loading control. (M–O) *apln* expression in the axial mesoderm and its derivative, notochord. (N) Cross-section through notochord. (P and Q) *apln* expression in the posterior notochord, prospective heart (ht), and within the head at 24 hpf. Animal pole, star; vegetal pole, number symbol; dorsal, D.

The scale bar represents 100 μm in (A), (I), (J), and (N) and 200 μm in (B), (D), (G), (H), (K), (M), (O), (P), and (Q).

(Figures 2K and 2L). Strikingly, at segmentation stages, the expression of *cmlc2* in cardiac precursors was strongly reduced or missing (Figures 3A, 3B, and 3G). At 2 dpf, a functional heart was not detected in the vast majority of *agtrl1b* morphant embryos, while the body length appeared normal (Figures 3D, 3E, and 3H). To test the specificity of this phenotype, we coinjected sequence-modified *agtrl1b* RNA (*agtrl1b*$^{MO\text{-}mut}$) that should not bind MO^{agtrl1b}. Indeed, 54% of the embryos coinjected with MO^{agtrl1b} and the MO-resistant RNA showed partial suppression of the MO^{agtrl1b}-dependent phenotype, exhibiting a small beating heart (Figure 3F). By contrast, 93% percent of the embryos injected with MO^{agtrl1b} alone failed to form a functional heart (Figure 3H). Consistently, 57% of these embryos coinjected with MO^{agtrl1b} and rescuing mRNA exhibited faint *cmlc2* staining, compared to 36% of the embryos that were injected with MO^{agtrl1b} alone (Figure 3G). The incomplete suppression of this phenotype may be explained in part by the observation that both expression of high doses of Agtrl1b (400 pg, Figure 3C) and depletion of Agtrl1b caused cardiac deficiency. Taken together, these experiments revealed an essential role of Agtrl1b in heart formation.

Deficiency and Excess Apelin Impair Gastrulation and Heart Formation

We next tested the involvement of the ligand Apelin in gastrulation and heart development. Excess Apelin impaired epiboly, a process that involves coordinated movements of the blastodermal layers toward the vegetal pole to enclose the yolk cell. In 73% (n = 122) of the embryos injected with 10 pg synthetic RNA encoding the Apelin prepropeptide (Lee et al., 2000), movement of the blastoderm toward the vegetal pole was delayed (Figures 2M and 2N). Moreover, dorsal forerunner cells, a small cell cluster that originates from the dorsal blastoderm margin

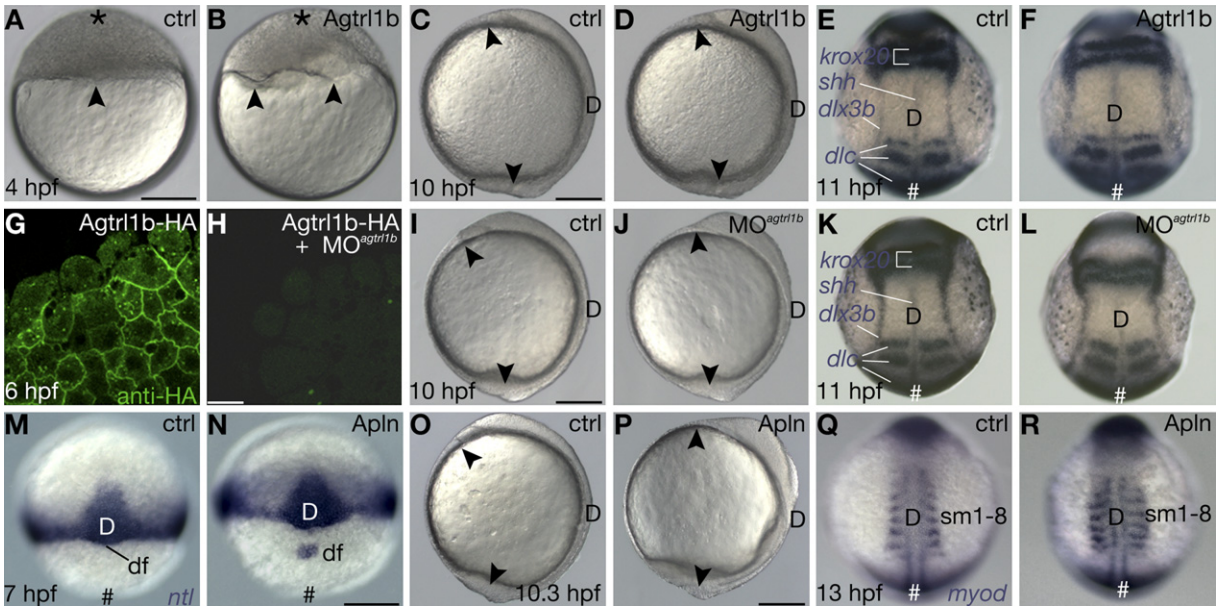

Figure 2. *agtrl1b* and *apelin* Can Influence Gastrulation Movements

(A–L) *agtrl1b* (A–F) gain-of-function and (G–L) loss-of-function experiments. (A and B) Agtrl1b misexpression (B) causes distortion at the interface between the blastoderm and the yolk cell at early epiboly, in contrast to the (A) smooth yolk surface, indicated by an arrowhead, in an uninjected control embryo. (C and D) (D) By the end of gastrulation, embryos overexpressing Agtrl1b show normal anteroposterior extension; arrowheads indicate the anterior and posterior limits of the nascent embryonic axis. (E and F) Tissue specification and patterning as revealed by *krox20* (hindbrain rhombomeres 3 and 5), *deltaC* (*dlc*, newly formed somites), *dlx3b* (neural-nonneural ectoderm boundary), and *shh* (notochord) expression. (F) These markers reveal mediolateral expansion of tissues, consistent with reduced convergence gastrulation movements in Agrl1b-misexpressing embryos. (G and H) Evaluation of $MO^{agtrl1b}$ effectiveness. Confocal microscopy image of cell membrane-localized HA-tagged Agtrl1b in blastulae injected with its synthetic RNA. (H) Coinjection of $MO^{agtrl1b}$ suppresses ectopic HA-tagged Agtrl1b expression. (I–L) Embryos injected with $MO^{agtrl1b}$ manifest a mild reduction of anteroposterior embryonic axis and a normal mediolateral expansion at the end of gastrulation. (K and L) Tissue specification and patterning, marked by *krox20*, *dlc*, *dlx3b*, and *shh* expression, are not affected.

(M–R) Effect of Apelin misexpression on early gastrulation. (M, O, and Q) Uninjected control embryos (ctrl). (N, P, and R) Embryos injected with 10 pg *apln* RNA (Apln). (M and N) Dorsal views at 7 hpf; the animal pole is oriented toward the top. *no tail* (*ntl*) expression in the mesoderm at the blastoderm margin/blastopore marks the progress of epibolic movements toward the vegetal pole (number symbol); (N) dorsal forerunner cells (df) are well separated in *apln* RNA-injected embryos, revealing impaired epiboly of the blastoderm margin. (O and P) Lateral view, 1-somite stage, 10.3 hpf. The anteroposterior axis, marked with arrowheads, is reduced in *apln* RNA-injected embryos. (Q and R) Dorsal view at the 8-somite stage; the animal pole is oriented (star) toward the top. (R) *myod* marks formed somites, which are expanded mediolaterally in *apln* RNA-injected embryos. Dorsal, D. The scale bar represents 5 μm in (H) and 200 μm in (A), (C), (I), (N), and (P).

and moves vegetally in front of the blastoderm, were well separated from the delayed blastoderm (Figures 2M and 2N). Hence, excess Apelin interferes with epibolic movements of most deep cells during gastrulation. During early segmentation, 91% (n = 221) of the embryos misexpressing Apelin showed reduction of the AP axis (Figures 2O and 2P) and mediolaterally expanded somites (Figures 2Q and 2R), suggesting that excess Apelin also impairs convergence and extension movements. However, tissue specification and patterning during gastrulation were not significantly altered (Figures 2Q and 2R and data not shown). At late segmentation, embryos misexpressing Apelin displayed a complete lack of the heart markers *nkx2.5* (Figures 4A and 4B), *cmlc2* (Figures 4C and 4D), and *ventricle myosin heavy chain* (*vmhc*) (Figures 4E and 4F), despite having relatively normal morphology and expression of *vmhc* in the somites (Figures 4E and 4F). Furthermore, these embryos did not exhibit a beating heart at 2 dpf (data not shown). At 30 hpf, embryos misexpressing Apelin also displayed reduced expression of several anterior LPM markers, including *hand2*, *gata5*, *tbx1*, as well as *nkx2.3* in pharyngeal pouch mesenchyme and *tbx5* in pectoral fin, indicating that other anterior LPM derivatives were affected (Figure S2 and data not shown).

To determine which developmental processes require Apelin, we designed MOs to interfere with either protein translation ($MO^{apln\text{-}atg}$) or RNA splicing ($MO^{apln\text{-}spl}$). Binding of $MO^{apln\text{-}spl}$ should cause an insertion of intron1-derived sequences predicted to create a premature stop codon following the first 27 amino acids of Apelin, which would therefore lack the carboxyl-terminal sequence essential for receptor binding and activation (Hosoya et al., 2000; Kawamata et al., 2001; Lee et al., 2000). Injection of 10 ng $MO^{apln\text{-}spl}$ was sufficient to suppress normal splicing of endogenous *apln* RNA, as revealed by RT-PCR at 12, 24, and 32 hpf (Figure 4G and data not shown). Moreover, $MO^{apln\text{-}atg}$ suppressed the epiboly defects caused by injection of *apln* RNA, but did not affect the phenotype

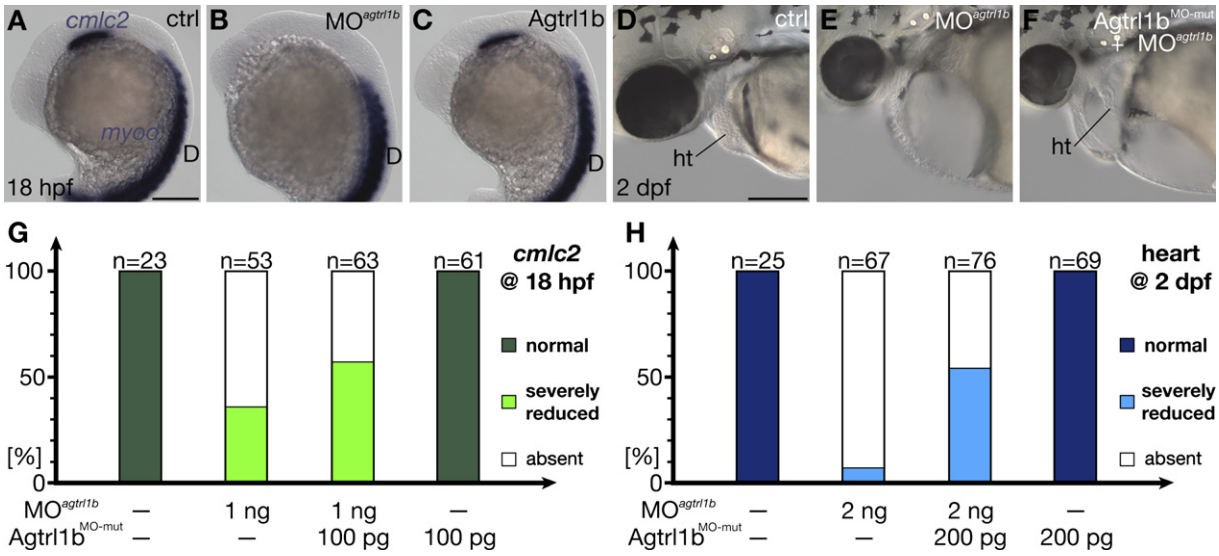

Figure 3. *agtrl1b* Is Essential for Heart Formation

(A–H) *agtrl1b* loss-of-function experiments. Downregulation of Agtrl1b expression causes deficiency of (B) cardiac precursors marked by *cmlc2*, compared to (A) an uninjected control embryo, without affecting somitic *myod* expression. (C) Ectopic Agtrl1b activity mildly impairs cardiac precursor development. (D and E) Functional heart (ht) does not form in *agtrl1b* morphant embryos, (F) but residual heart is observed in embryos coinjected with $MO^{agtrl1b}$ and 200 or 100 pg MO-resistant synthetic *agtrl1b* RNA. (G–H) Evaluation of $MO^{agtrl1b}$ specificity scored by (G) *cmlc2* expression at mid-segmentation or (F and H) morphology at 2 dpf. Dorsal, D. The scale bar represents 100 μm in (D)–(F) and 200 μm in (A)–(C).

caused by a mutated form of the *apln* RNA that lacked sequences for $MO^{apln\text{-}atg}$ binding (data not shown).

Embryos injected with either 1 ng $MO^{apln\text{-}atg}$ or 10 ng $MO^{apln\text{-}spl}$ exhibited the same phenotype, characterized by reduced expression of myocardial markers, including *cmlc2* (84%, n = 63, and 81%, n = 62, respectively) and *vmhc* (83%, n = 58, and 96%, n = 45, respectively) (Figures 4H–4M and not shown), despite normal *vmhc* expression in the somites (Figures 4J and 4K). However, the $MO^{apln\text{-}spl}$ embryos showed neither a delay in the fusion of bilateral heart primordia (Figures 4L and 4M) nor cardia bifida at 1 dpf (data not shown).

Apelin Signals through Agtrl1b during Gastrulation

Since interference with Apelin or Agtr1b impaired cardiac precursor formation, we asked whether Apelin signals via the Agtrl1b receptor in zebrafish embryos, as reported for its mammalian homologs (Lee et al., 2000; Tatemoto et al., 1998). We reasoned that the ligand and its receptor should have synergistic effects on development in coinjection experiments. Accordingly, embryos injected separately with low doses of synthetic RNAs encoding Agtrl1b or Apelin progressed through gastrulation, whereas embryos co-injected with the same doses of both RNAs underwent developmental arrest by late blastula stages and most died by 1 dpf (Figures 5A–5E). We also expected that Agtrl1b function should be required for excess Apelin to impair gastrulation movements. Accordingly, injections of $MO^{agtrl1b}$ significantly suppressed the epiboly delay caused by Apelin misexpression (Figures 5F–5J). Together, these results provide strong support for the notion that during zebrafish gastrulation Apelin functions upstream of the Agtrl1b receptor, likely as its specific ligand.

Deficiency or Excess Apelin Impairs Convergence and Extension Movements of Anterior LPM and Heart Precursors

The deficiency of cardiac gene expression in embryos with reduced or excess Apelin could result from loss of a localized source of Apelin signal to guide the cardiac precursors to the correct location. Indeed, guided cell migration can be compromised by both a deficit and an excess of cues (Doitsidou et al., 2002; Duchek and Rorth, 2001; Solnica-Krezel, 2005). Alternatively, loss of heart precursors could reflect defective cell fate specification or survival. To address these possibilities, we performed cell-tracing experiments (Figures 6A–6J; Figures S3A–S3D) (Sepich and Solnica-Krezel, 2005). Mesendodermal cell groups at the lateral blastoderm margin that give rise to the cardiac precursors (Keegan et al., 2004) were labeled by photoactivation of caged fluorescein at the beginning of gastrulation (Figures 6A and 6B). The embryos were fixed during segmentation, and the labeled cells were visualized with anti-fluorescein antibody, while somitic and heart precursors were detected by using antisense RNA probes (*myod* and *cmlc2*, Figures 6C, 6D, 6F, and 6G; *deltaC*, Figures S3A–S3D). In control embryos, as previously described for convergence and extension movements of the lateral mesoderm (Myers et al., 2002), the labeled cell populations converged toward the midline and extended from the tail, through the heart field, and to the most anterior part of the embryo, forming a fine stripe

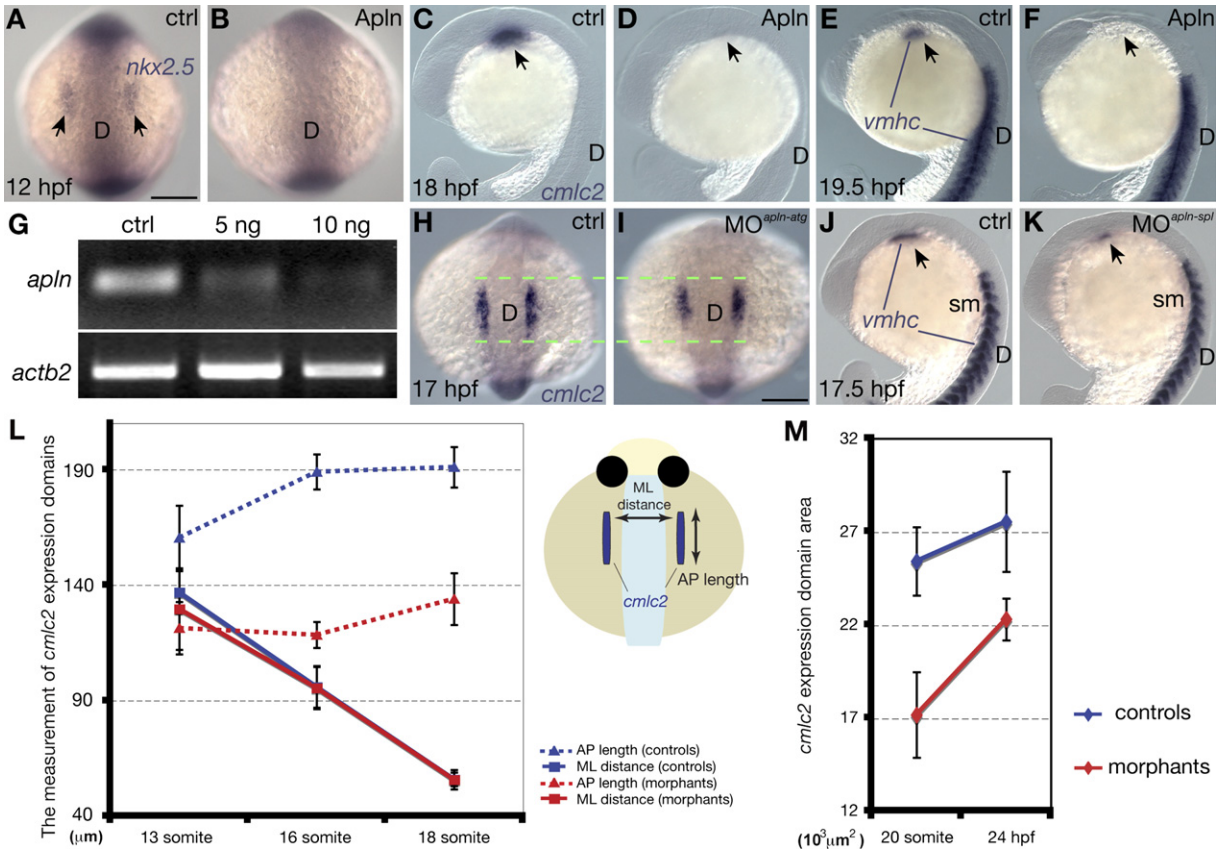

Figure 4. Excess and Deficiency of Apelin Impair Heart Formation

(A–M) *apelin* (A–F) gain-of-function and (G–M) loss-of-function experiments. (A, C, E, H, and J) Control embryos (ctrl). (B, D, and F) Embryos injected with 10 pg *apln* RNA (Apln). (I) Embryos injected with 1 ng MO$^{apln\text{-}atg}$. (K) Embryos injected with 10 ng MO$^{apln\text{-}spl}$. (A and B) Dorsal view; *nkx2.5* expression in cardiac precursors (arrows) is not detected in Apelin-misexpressing embryos at midsegmentation. (C–F) Expression of (C) *cmlc2* (arrow) and (E) *vmhc* (arrow) in heart primordia of late segmentation control embryos is not detected in (D and F) Apelin-misexpressing siblings (arrows). (E and F) Normal *vmhc* expression in somites (sm) of control and Apelin-misexpressing siblings. (G) RT-PCR-amplified *apln* fragment from uninjected embryos (lane ctrl) at 32 hpf, and embryos injected with *apln* MO$^{apln\text{-}spl}$ at 5 ng and 10 ng doses. *β-actin 2* (*actb2*) was used as a loading control. (H–K) Reduced expression of the cardiac markers *cmlc2* and *vmhc* (arrows), but not somitic *vmhc* expression (sm), in embryos depleted of Apelin by MO$^{apln\text{-}atg}$ or MO$^{apln\text{-}spl}$. Dorsal, D. The scale bar represents 200 μm in (A) and (I). (L) Measurement of the anteroposterior dimension and the mediolateral distance between the two *cmlc2* expression domains in uninjected control embryos and *apln*^{spl} morphants at three developmental stages before the fusion of cardiac primordia (13, 16, and 18 somite). AP, anteroposterior; ML, mediolateral. (M) After bilateral heart primordia fused together, the area of the *cmlc2* expression domain was measured at the 20-somite stage and 24 hpf in control and *apln*^{spl} morphant embryos. Each point represents the average measurement of ten embryos. Error bars depict standard deviation.

(n = 37, Figures 6C and 6D; Figures S3A and S3B). Measurements revealed that the labeled cell array extended 886.5 ± 54.3 μm from the eighth somite to the anterior end (n = 19; Figure S3A). In contrast, in embryos injected with 10 pg synthetic *apln* RNA, the labeled cell population converged to the dorsal midline and reached a comparable position within the tail, but it failed to extend anteriorly and to express *cmlc2* (n = 44, Figures 6F and 6G; Figures S3C and S3D). The length of the stripes formed by the labeled cells extending anterior to the eighth somite was significantly shorter than in controls (Figure S3C, 310.2 ± 51.3 μm; n = 15; $p < 0.0001$), revealing an extension defect. We interpret these fate-mapping assays to indicate that in embryos misexpressing Apelin, anterior LPM cells including the cardiac precursors, failed to move to the correct location in the embryo and consequently failed to undergo proper cell fate specification, as demonstrated by the lack of heart marker expression.

Next, we asked whether heart field reduction in Apelin-deficient embryos was associated with defective cell movements. As described above, in gastrulae depleted of Apelin by MO$^{apln\text{-}spl}$, lateral mesodermal cell populations were labeled by photoactivation of caged fluorescein (Figures 6A and 6B). By early segmentation, these cells formed stripes that extended from the head to the tail, as in control experiments (Figures 6I and 6J). Analysis of tissue-specific markers (*shh* and *deltaC*) revealed a mediolaterally broadened notochord and somites in Apelin morphants, consistent with mild convergence defects of all mesodermal tissues. Strikingly, the anterior portion of

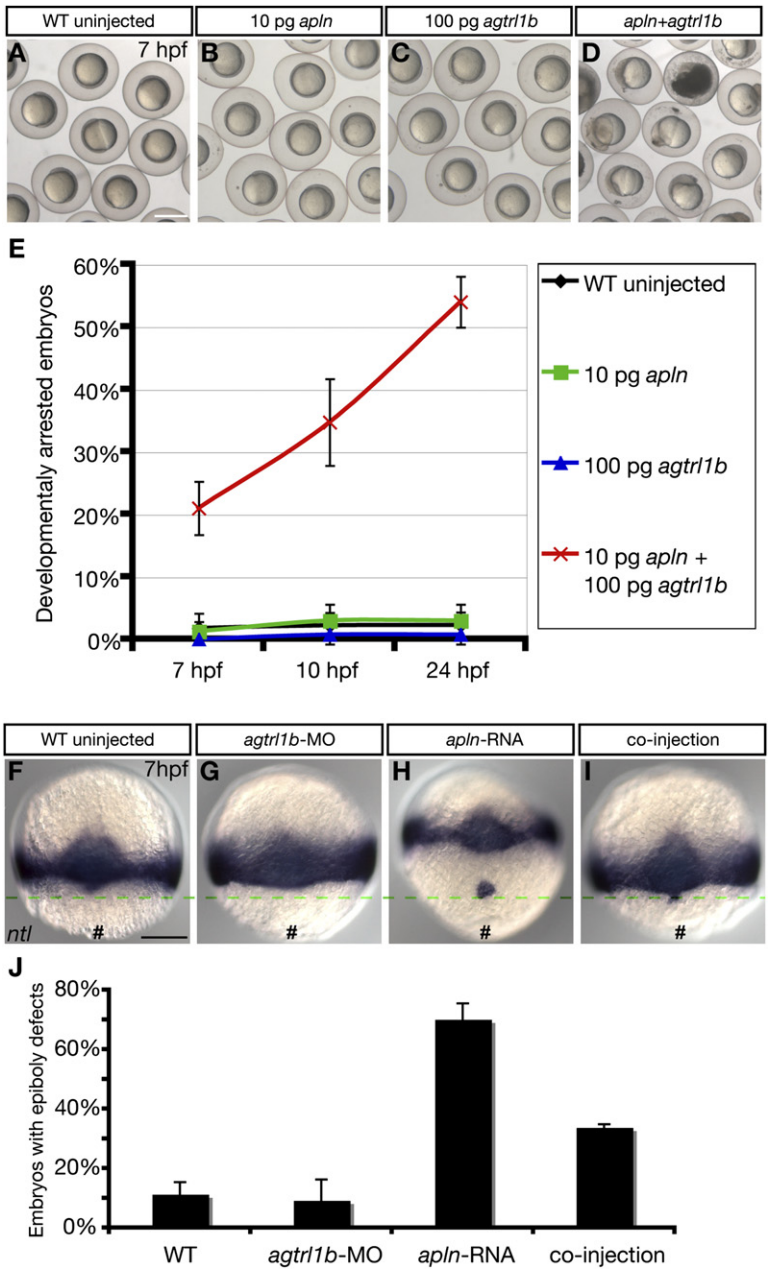

Figure 5. Functional Interaction of Apelin and Agtrl1b during Zebrafish Gastrulation

(A–E) Coinjection of synthetic *apln* and *agtrl1b* RNAs leads to developmental arrest in a synergistic fashion. (B and C) Injection of low doses of synthetic *apln* and *agtrl1b* RNAs alone rarely caused developmental arrest, as observed for (A) uninjected wild-type embryos. (D) Embryos coinjected with the same doses of synthetic *apln* and *agtrl1b* RNAs underwent developmental arrest by late blastula stages. (E) The graph shows the fraction of developmentally arrested embryos at different times after fertilization in the above-desribed experiments. Data are from three separate experiments: uninjected wild-type embryos (n = 213), 10 pg *apln* RNA-injected embryos (n = 199) and 100 pg *agtrl1b* RNA-injected embryos (n = 189), and embryos coinjected with 100 pg *agtrl1b* RNA and 10 pg *apln* RNA (n = 194). Error bars depict standard deviation.

(F–J) Injection of *agtrl1b* MO suppresses epiboly defects caused by ectopic Apelin expression. Top panel, *no tail* (*ntl*) expression marks the mesendodermal margin and dorsal forerunner cells in (F) uninjected control embryos, (G) 2 ng $MO^{agtrl1b}$-injected embryos, (H) 10 pg *apln* RNA-injected embryos, and (I) 2 ng $MO^{agtrl1b}$ and 10 pg *apln* RNA coinjected embryos. Dorsal forerunner cells are tightly associated with the blastoderm margin in (F) uninjected wild-type and (G) $MO^{agtrl1b}$-injected embryos, while (H) embryos overexpressing Apelin exhibit defective epiboly, demonstrated by the separation of dorsal forerunner cells from the blastoderm margin and delayed movement of the margin toward the vegetal pole. (I) An embryo coinjected with *apln* RNA and $MO^{agtrl1b}$ shows a significant suppression of the epiboly defect. (J) The graph depicts the percentage of embryos with epiboly defects, assessed by *ntl* staining. Data are from three separate experiments: uninjected wild-type embryos (n = 83), 2 ng $MO^{agtrl1b}$-injected embryos (n = 59) and 10 pg *apln* RNA-injected embryos (n = 65), and embryos coinjected with 2 ng $MO^{agtrl1b}$ and 10 pg *apln* RNA (n = 69).

Error bars depict standard deviation. Vegetal pole, number symbol. The scale bar represents 200 μm in (F) and 600 μm in (A).

the labeled cell arrays was positioned much further from the midline in the Apelin morphants compared to control embryos (Figures 6I–6L). This effect was quantified at the first somite, where the labeled cell array was positioned in a more lateral somite region than in control embryos (Figures 6K and 6L). This result indicates that convergence movements of the lateral mesoderm cells are more severely compromised than movements of other mesodermal tissues, revealing a specific requirement for Apelin in convergence movements of anterior LPM.

By midsegmentation, the labeled cell arrays converged toward the midline in morphants (n = 10/10, Figure 6H; and $MO^{apln\text{-}atg}$ not shown), similar to what is seen with control embryos (n = 8/8, Figure 6E). Notably, in the region of the heart field, these cell arrays were discontinuous and broader, in contrast to continuous and narrow stripes in the heart fields of control embryos (Figures 6E and 6H). Moreover, in Apelin morphants, some labeled cells were found in ectopic positions on both sides of the array, even on the opposite side of the midline (n = 9/10, Figure 6H), in contrast to what is seen with control embryos (0/8). Together, these studies demonstrate that both an excess and deficit of Apelin impair migration of the anterior LPM cells during late gastrulation.

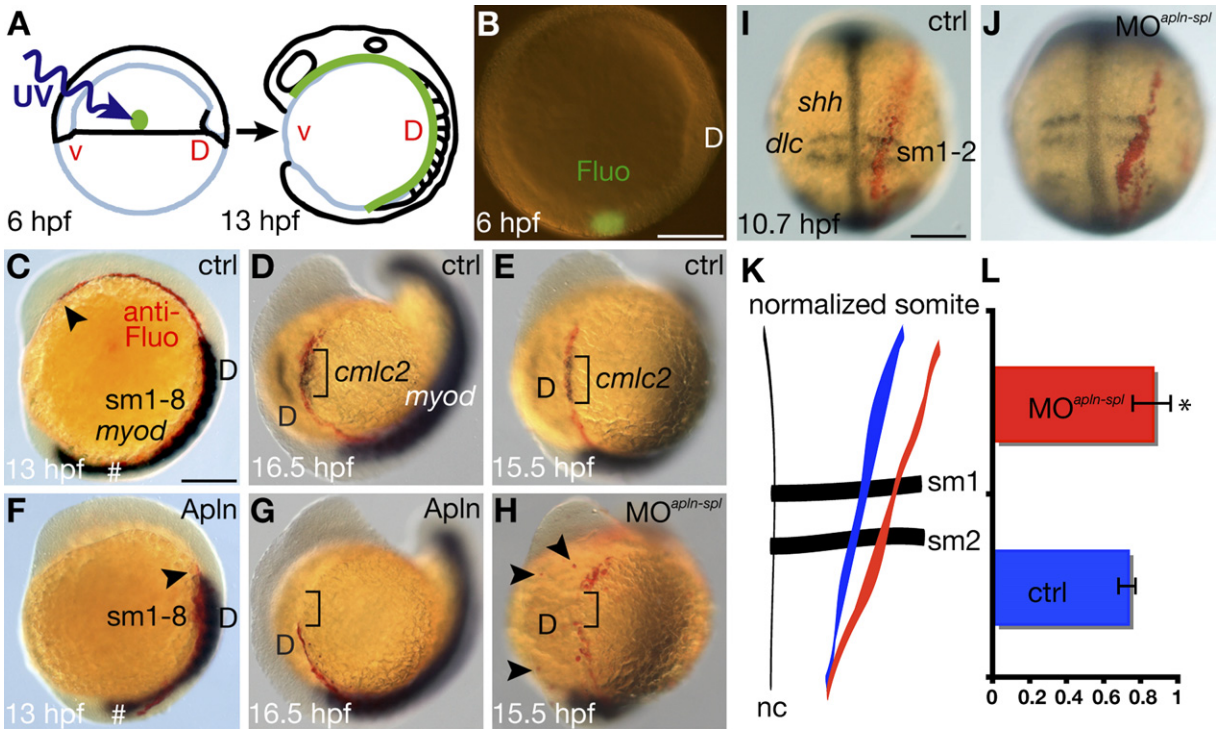

Figure 6. Abnormal Convergence and Extension Movements of Lateral Mesoderm Cells in Embryos with Reduced and Excess Apelin

(A) The method for labeling cell populations by photoactivation of caged FITC-dextran is illustrated. A prospective mesodermal cell population is labeled at the lateral blastoderm margin at the start of gastrulation (6 hpf). The labeled cell group is followed through gastrulation as it elongates and converges toward the dorsal midline and extends anteroposteriorly.

(B) Image of an embryo with the animal pole oriented toward the top and dorsal oriented toward the right in which a group of labeled cells positioned 90° from the dorsal midline is visualized under the fluorescent channel and Nomarski optics.

(C–L) (C–H, I, and J) Tracing fates and movements of the lateral mesoderm cells in (C, D, E, and I) uninjected control embryos and in embryos with (F and G) an excess and (H and J) a deficit of Apelin. (C and F) Lateral views, (I and J) dorsal views, and (D, G, E, and H) dorsoanterior views at the (I and J) 2-somite, (C and F) 8-somite, (E and H) 13-somite, and (D and G) 15-somite stages. Photoactivated cells are revealed with an anti-Fluorescein antibody (red). The somitic expression of *myod*, *deltaC* (*dlc*), and *shh* in notochord visualized in blue provides landmarks and also staging information. The (C) labeled cell population undergoes strong extension from head to tail in control embryos, while rostral extension of the (D and E) labeled cell population is suppressed in (F) Apln-misexpressing embryos. In (D and E) control embryos, the anterior labeled cell population overlaps with *cmlc2*-expressing cardiac precursors, whereas in (G) Apelin-misexpressing embryos, rostral extension of the labeled cell population is suppressed and *cmlc2* expression is missing; in (H) Apelin morphants (10 ng $MO^{apln\text{-}spl}$), labeled cells are distributed discontinuously in the heart field region and outside the stripe. (I–L) At the 2-somite stage in the (J) Apelin morphants, labeled anterior mesoderm cells are positioned much further from the midline, and somites are broadened compared to (I) control embryos. (K) Depiction of the relative position within the somite of mesodermal cell populations labeled by photoactivation 95° from dorsal at the onset of gastrulation in Apelin morphant (red stripe) and uninjected control embryo (blue stripe). The somite width was normalized between the control and Apelin morphant embryos. (L) Quantification of the relative position of the labeled cell populations at the first somite, demonstrating that the labeled cell array was positioned in a more lateral somite region of Apelin morphants compared to control embryos. Five uninjected control embryos (0.721 of the normalized somite, SD = ±0.0464) and nine morphants embryos (0.854 of the normalized somite, SD = ±0.1029) were analyzed at 10.7 hpf.

Error bars depict standard deviation. *$p < 0.001$. The scale bar represents 200 μm in (B), (C), and (I). Vegetal pole, number symbol; dorsal, D; ventral, v.

Abnormal Cell Movement Behaviors in Gastrulae with Reduced and Excess Apelin

To determine whether the inhibited anterior movements of heart precursors in Apelin-overexpressing embryos were associated with abnormal cell behaviors, we carried out time-lapse analyses at midgastrulation stages. Consistent with gene expression and cell-tracing analyses (Figures 2M, 2N, 6C, 6D, 6F, and 6G; Figure S3), the width of the mesendoderm, from the anterior edge to the margin, was reduced, confirming that both the epibolic and anterior mesendoderm movements were inhibited (Figures 7A and 7D; Movie S1). Cell tracking further demonstrated that the anteriorward migration of mesendodermal cells was impaired (Figures 7B and 7E; Movie S1) and revealed the associated cellular defects. In normally developing control embryos injected with synthetic RNA encoding a truncated form of Apelin (AplnΔ13) incapable of being secreted, mesendodermal cells were elongated and pear shaped. This contrasted rounder cell shapes in Apelin-misexpressing gastrulae (Figures 7C, 7F, and 7I). Mesodermal cells in the control gastrulae formed and maintained one predominant filolamellipodial protrusion

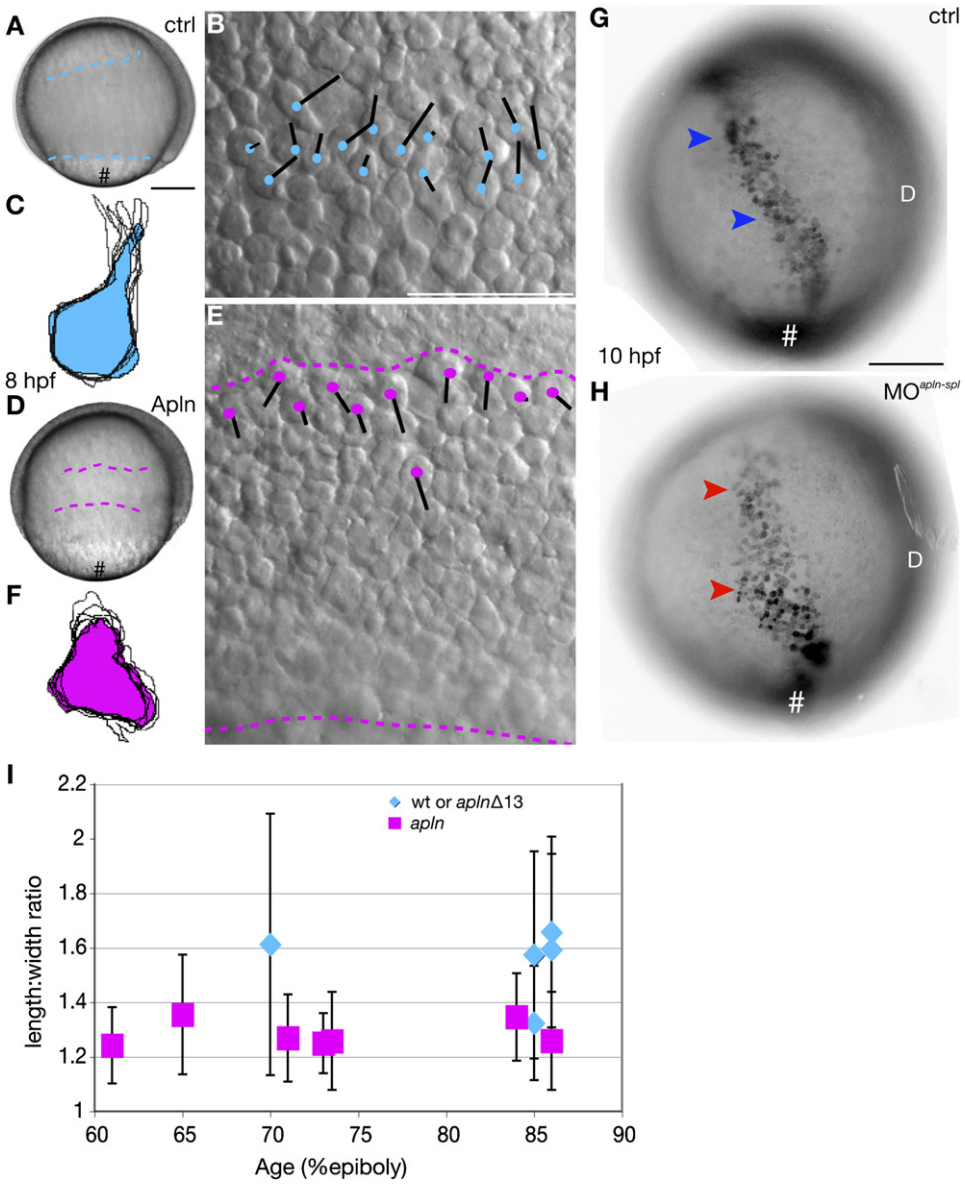

Figure 7. Time-Lapse Data Reveal Abnormal Cell Behaviors of Lateral Mesoderm Cells in Embryos with Reduced and Excess Apelin

(A–F) Time-lapse data at midgastrula stages from control (A–C) *apln∆13* RNA-injected and (D–F) *apln* RNA-injected embryos. (A and D) In lateral views, the anterior and posterior edges of the lateral mesendoderm are marked with dotted lines. (B and E) Net paths of mesodermal cells over 36 min, from embryos depicted in (A) and (D), respectively. (C and F) Mesodermal cells in control (C) ApelinΔ13-expressing gastrulae exhibit an elongated pear shape with one predominant lamellae, whereas (F) Apelin-overexpressing mesodermal cells are rounder and form blebs. Drawings show outlines of cells at 10 s intervals for 1 min.

(G and H) Labeled lateral mesodermal cells from (G) control and (H) $MO^{apln\text{-}spl}$-injected siblings at late gastrulation stages show disrupted cell movements when *apln* is depleted. Cell arrays are more dispersed (red arrowheads) in *apln* morphant embryos (n = 2) than those in uninjected control embryos (blue arrowheads) (n = 2).

(I) Cell polarity defects in Apelin-overexpressing embryos. Lateral mesodermal cells in Apelin-overexpressing gastrulae exhibit rounder shapes, as revealed by determining the length-to-width ratio (LWR) of mesodermal cells at several stages during gastrulation. Each point represents the average LWR of 20 cells from 1 embryo.

Error bars depict standard deviation. The scale bar represents 50 μm in (B) and 200 μm in (A) and (G). Vegetal pole, number symbol; dorsal, D.

at a time, as expected for cells undergoing directed migration (Figure 7C; Movie S2). In contrast, cells in embryos with excess Apelin extended fewer filolamellipodia, and they instead formed bleb-like protrusions (Figure 7F; Movie S3). Overall, mesendodermal cells in Apelin-misexpressing embryos were less able to maintain a polarized morphology typical of migrating cells (Vicente-Manzanares et al., 2005).

To ask how the loss of Apelin function affects cell movements, we carried out similar time-lapse recordings of labeled anterior LPM cells in embryos depleted of Apelin by $MO^{apln\text{-}spl}$ at late gastrulation (Movies S4–S7). Whereas in the control gastrulae labeled LPM cells formed stripes that narrowed over time, in morphants the stripes appeared to narrow less or/and to fragment (Figures 7G and 7H; Movies S4–S7, n = 2 control, n = 2 *apln* morphant). Together with our fate-mapping experiments (Figures 6E, 6I, 6H, and 6J), these time-lapse analyses reveal impaired migration of LPM cells in Apelin-deficient embryos.

Increased Cell Death Does Not Account for Heart Deficiency in Embryos with Abnormal Apelin/Agtrl1b Signaling

To determine whether cell death could account for the loss of heart cells in Apelin/Agtrl1b-deficient embryos, we first detected apoptotic cells by using TUNEL staining (Mizumatsu et al., 2003). We observed increased cell death in the animal half of the *apelin* and *agtrl1b* morphant embryos at the 8-somite stage, when heart field was reduced (Figures S4A, S4B, S4E, and S4F and data not shown). However, the amount of cell death did not correlate with the severity of heart loss: we observed a level of cell death in *agtrl1b* morphants (where heart was strongly reduced) that was comparable to that in *apelin* morphants (with much milder reduction of the heart field, Figure S4 and data not shown). Second, we inhibited apoptosis by coinjecting a MO against p53 (Campbell et al., 2006) along with $MO^{apln\text{-}spl}$. While this significantly reduced cell death in both control and *apelin* morphant embryos, it did not suppress deficiency of heart precursors, as assayed by *cmlc2* expression at 15.5 hpf and 17 hpf (Figures 4L and 4M; Figures S4B, S4D, S4F, S4H, and S4I). These results argue against the notion that the reduction of heart field in Apelin/Agtrl1b-deficient embryos is primarily due to increased cell death. However, we cannot exclude the possibility that effects on survival may also contribute to the phenotype observed in embryos with reduced Apelin/Agtrl1b signaling.

We addressed further cell fate specification, by monitoring the earliest cardiac fates in Apelin-overexpressing embryos, by using *hand2, gata5*, or *tbx1*. We found that these genes exhibited in the anterior LPM reduced and patchy expression, which correlated with noncardiac cell fate populations (Figure S2 and data not shown). These results indicate that excess Apelin signaling inhibits heart fate, either by directly impairing fate specification of heart precursors or indirectly by strongly impairing their migration and disrupting inductive interactions along the normal route.

DISCUSSION

Here, we provide several lines of evidence that gastrulation movements of anterior LPM and heart precursors in particular are highly sensitive to the level and distribution of Apelin and Agtrl1b expression. Moreover, epistasis experiments and the observation that Apelin and Agtrl1b have synergistic effects on zebrafish development in coexpression experiments provide strong support for the notion that during zebrafish gastrulation Apelin functions upstream of the Agtrl1b receptor, likely as its specific ligand.

How does Apelin/Agtrl1b signaling regulate movements of cardiac progenitors? Our analyses suggest that Apelin does not simply act as a chemoattractant or chemorepellant. Based on the following observations it is tempting to speculate that Apelin might have concentration-dependent effects on cardiac precursor cell movements. First, cardiac precursors converge toward the *apln*-expressing midline during gastrulation, but they stop short of reaching the midline to form bilateral fields at early segmentation (Keegan et al., 2004). We observed a delayed convergence of the LPM during gastrulation in Apelin-deficient embryos (Figures 6I–6L), and more dispersed and ectopic distribution of anterior LPM cells, including heart precursors at midsegmentation (Figures 6E and 6H), whereas global overexpression of Apelin strongly inhibited some of the gastrulation movements of mesodermal cells. In this scenario, Apelin emanating from the midline would initially attract heart precursors until they moved near the midline to experience a higher and inhibitory concentration of Apelin. It is also possible that Apelin/Agtrl1b signaling has a permissive role in cardiac progenitor migration during gastrulation, as suggested for S1P-Miles apart GPCR signaling, which is essential for the migration of bilateral heart primordia to the midline during segmentation (Kupperman et al., 2000). Other roles of Apelin, such as promoting adhesion of cardiac precursors to each other or to substratum as they coalesce into the bilateral heart primordia, are also possible (Hashimoto et al., 2005).

That the convergence defect in *apln* morphants of the labeled anterior LPM cells, except the heart precursors, was corrected during segmentation (Figures 6J and 6K) is likely due to redundant signals guiding these cells. Indeed, *silberblick (wnt11)* mutants that manifest severe convergence and extension defects at late gastrulation acquire a more normal body elongation by segmentation stages due to expression of the *pipetail/wnt5* gene with overlapping activity (Heisenberg et al., 1996; Kilian et al., 2003). The persistent movement defect of heart precursors in embryos with an excess or a deficit of Apelin suggests that these cells are particularly sensitive to the level and distribution of Apelin. This enhanced sensitivity of heart precursors to Apelin/Agtrl1b signaling is puzzling given that Agtrl1b is expressed broadly in the anterior LPM and ventroposterior mesoderm during late gastrulation (Figure 1). However, expression of a GPCR beyond its target tissue has been previously reported. The GPCR CXCR-4, which guides the migration of primordial germ cells, is expressed throughout the mesoderm at the onset of gastrulation, yet the loss of CXCR-4 function disrupts only the migration of germ cells without interfering with gastrulation movements of mesodermal cells (Doitsidou et al., 2002; Knaut et al., 2003).

Together, our results reveal a requirement for the GPCR Agtrl1b and its ligand, Apelin, in heart field formation,

through regulation of convergence and extension gastrulation movements of cardiac precursors in zebrafish. Significantly and in contrast to global regulators of gastrulation movements, such as noncanonical Wnt signaling, prostaglandins, and Stat3 (Keller, 2005; Solnica-Krezel, 2005), Apelin signaling has a more restricted role in regulating movements of the anterior LPM cells and heart precursors in particular. We speculate that the Apelin/Agtrl1b axis provides just the first example of GPCRs regulating gastrulation movements of defined cell populations to form organ rudiments during vertebrate embryogenesis.

EXPERIMENTAL PROCEDURES

Zebrafish Husbandry

Zebrafish (*Danio rerio*) were maintained as described previously (Solnica-Krezel et al., 1994). Embryos were staged according to Kimmel et al. (1995).

In Situ Hybridization, Immunohistochemistry, and Histology

Single- and double-color whole-mount in situ hybridization were performed essentially as described previously (Thisse et al., 1993); BM Purple (Roche) and INT/BCIP (175 μg/ml; Roche) were used as alkaline phosphatase substrates. The following molecular markers were used: *nkx2.5*, *cmlc2*, and *vmhc* (for original references, see Yelon and Stainier [1999]), and *krox20*, *shh*, *dlx3b*, *dlc*, *ntl*, and *myod* (for original references, see Sepich and Solnica-Krezel [2005]).

Lineage Tracing

Embryos were microinjected at the 1-cell stage with *agtrl1b* or *apln* synthetic capped RNA (Marlow et al., 1998), with *agtrl1b*, or with *apln*-specific MOs ($MO^{agtrl1b}$, 5′-CAGAGAAGTTGTTTGTCATGTG CTC-3′ [CV109234]; $MO^{apln\text{-}spl}$, 5′-AACAGCCGTCACGCTCCCGACTT AC-3′ [DQ062434]; $MO^{apln\text{-}atg}$, 5′-TTCTGCTCTCCCCTCCGTTTCCC TG-3′ [DQ062434]; Open Biosystems). A mutant form of *agtrl1b* (*agtrl1b*$^{MO\text{-}mut}$), predicted to be unable to bind $MO^{agtrl1b1}$, was constructed by using the following primers: forward, 5′-GGAATGAAT GCCATGGACAAC-3′; reverse, 5′-CCAATTCTGCGTCACCCTTC-3′. In coinjection experiments, each reagent was microinjected independently at the 1-cell stage. Injection and photoactivation of anionic dextran DMNB caged fluorescein (Molecular Probes, D-3310) was performed as described (Sepich et al., 2000; Sepich and Solnica-Krezel, 2005).

Microscopy

Embryos stained by whole-mount in situ hybridization were mounted in 80% glycerol/PBT and were photographed with a Zeiss Axiophot microscope and an Axiocam digital camera. Live embryos were anesthetized if needed and were mounted in 1.5% or 2.5% methylcellulose. Images were made by using Photoshop and Illustrator software (Adobe).

Time-Lapse Analysis

Nomarski time-lapse images were collected as described (Myers et al., 2002). Multifocal plane recordings of the lateral mesoderm (90° from the dorsal midline) were collected from 60%–95% epiboly at 5 or 60 s intervals by using a 40× or 20× objective, respectively, on an Axiovert200M microscope (Carl Zeiss MicroImaging) with a Retiga EX*i* camera (Q Imaging). Fluorescent time-lapse embryos were mounted in 3% agarose wells filled with 2% methylcellulose (both in Danieau's buffer). Image collection and analysis were performed with OpenLab software (Improvision). Additional analysis was performed with Object-Image software (Norbert Vischer, http://simon.bio.uva.nl/object-image.html) and Excel (Microsoft).

Statistical Analysis

Calculations were made in Microsoft Excel. We report mean and standard deviation, the probability associated with the Student's t test (with two-tailed distribution), and two samples of unequal variance.

Supplemental Data

Supplemental Data include four figures, seven movies, and Supplemental Experimental Procedures and are available at http://www.developmentalcell.com/cgi/content/full/12/3/391/DC1/.

ACKNOWLEDGMENTS

We thank members of the L.S.-K. group for discussions and E. Raz, F. Marlow, and D. Yelon for critical comments. We thank I. Scott and D. Stainier for sharing results before publication and J. Clanton, H. Beck, and A. Bradshaw for excellent fish care. This work was supported by grants GM55101 and GM77770 from the National Institutes of Health.

Received: September 16, 2006
Revised: December 16, 2006
Accepted: January 17, 2007
Published: March 5, 2007

REFERENCES

Auman, H.J., and Yelon, D. (2004). Vertebrate organogenesis: getting the heart into shape. Curr. Biol. *14*, R152–R153.

Berry, M.F., Pirolli, T.J., Jayasankar, V., Burdick, J., Morine, K.J., Gardner, T.J., and Woo, Y.J. (2004). Apelin has in vivo inotropic effects on normal and failing hearts. Circulation *110*, II187–II193.

Campbell, W.A., Yang, H., Zetterberg, H., Baulac, S., Sears, J.A., Liu, T., Wong, S.T., Zhong, T.P., and Xia, W. (2006). Zebrafish lacking Alzheimer presenilin enhancer 2 (Pen-2) demonstrate excessive p53-dependent apoptosis and neuronal loss. J. Neurochem. *96*, 1423–1440.

Chen, M.M., Ashley, E.A., Deng, D.X., Tsalenko, A., Deng, A., Tabibiazar, R., Ben-Dor, A., Fenster, B., Yang, E., King, J.Y., et al. (2003). Novel role for the potent endogenous inotrope apelin in human cardiac dysfunction. Circulation *108*, 1432–1439.

Devic, E., Paquereau, L., Vernier, P., Knibiehler, B., and Audigier, Y. (1996). Expression of a new G protein-coupled receptor X-msr is associated with an endothelial lineage in *Xenopus laevis*. Mech. Dev. *59*, 129–140.

Devic, E., Rizzoti, K., Bodin, S., Knibiehler, B., and Audigier, Y. (1999). Amino acid sequence and embryonic expression of msr/apj, the mouse homolog of *Xenopus* X-msr and human APJ. Mech. Dev. *84*, 199–203.

Devreotes, P., and Janetopoulos, C. (2003). Eukaryotic chemotaxis: distinctions between directional sensing and polarization. J. Biol. Chem. *278*, 20445–20448.

Doitsidou, M., Reichman-Fried, M., Stebler, J., Koprunner, M., Dorries, J., Meyer, D., Esguerra, C.V., Leung, T., and Raz, E. (2002). Guidance of primordial germ cell migration by the chemokine SDF-1. Cell *111*, 647–659.

Duchek, P., and Rorth, P. (2001). Guidance of cell migration by EGF receptor signaling during *Drosophila* oogenesis. Science *291*, 131–133.

Habata, Y., Fujii, R., Hosoya, M., Fukusumi, S., Kawamata, Y., Hinuma, S., Kitada, C., Nishizawa, N., Murosaki, S., Kurokawa, T., et al. (1999). Apelin, the natural ligand of the orphan receptor APJ, is abundantly secreted in the colostrum. Biochim. Biophys. Acta *1452*, 25–35.

Hashimoto, Y., Ishida, J., Yamamoto, R., Fujiwara, K., Asada, S., Kasuya, Y., Mochizuki, N., and Fukamizu, A. (2005). G protein-coupled APJ receptor signaling induces focal adhesion formation and cell motility. Int. J. Mol. Med. *16*, 787–792.

Heisenberg, C.P., Brand, M., Jiang, Y.J., Warga, R.M., Beuchle, D., van Eeden, F.J., Furutani-Seiki, M., Granato, M., Haffter, P., Hammerschmidt, M., et al. (1996). Genes involved in forebrain development in the zebrafish, *Danio rerio*. Development *123*, 191–203.

Hosoya, M., Kawamata, Y., Fukusumi, S., Fujii, R., Habata, Y., Hinuma, S., Kitada, C., Honda, S., Kurokawa, T., Onda, H., et al. (2000). Molecular and functional characteristics of APJ. Tissue distribution of mRNA and interaction with the endogenous ligand apelin. J. Biol. Chem. *275*, 21061–21067.

Inui, M., Fukui, A., Ito, Y., and Asashima, M. (2006). Xapelin and Xmsr are required for cardiovascular development in *Xenopus laevis*. Dev. Biol. *298*, 188–200.

Kawamata, Y., Habata, Y., Fukusumi, S., Hosoya, M., Fujii, R., Hinuma, S., Nishizawa, N., Kitada, C., Onda, H., Nishimura, O., and Fujino, M. (2001). Molecular properties of apelin: tissue distribution and receptor binding. Biochim. Biophys. Acta *1538*, 162–171.

Keegan, B.R., Meyer, D., and Yelon, D. (2004). Organization of cardiac chamber progenitors in the zebrafish blastula. Development *131*, 3081–3091.

Keller, R. (2005). Cell migration during gastrulation. Curr. Opin. Cell Biol. *17*, 533–541.

Kilian, B., Mansukoski, H., Barbosa, F.C., Ulrich, F., Tada, M., and Heisenberg, C.P. (2003). The role of Ppt/Wnt5 in regulating cell shape and movement during zebrafish gastrulation. Mech. Dev. *120*, 467–476.

Kimmel, C.B., Ballard, W.W., Kimmel, S.R., Ullmann, B., and Schilling, T.F. (1995). Stages of embryonic development of the zebrafish. Dev. Dyn. *203*, 253–310.

Knaut, H., Werz, C., Geisler, R., and Nusslein-Volhard, C. (2003). A zebrafish homologue of the chemokine receptor Cxcr4 is a germ-cell guidance receptor. Nature *421*, 279–282.

Kupperman, E., An, S., Osborne, N., Waldron, S., and Stainier, D.Y. (2000). A sphingosine-1-phosphate receptor regulates cell migration during vertebrate heart development. Nature *406*, 192–195.

Lee, D.K., Cheng, R., Nguyen, T., Fan, T., Kariyawasam, A.P., Liu, Y., Osmond, D.H., George, S.R., and O'Dowd, B.F. (2000). Characterization of apelin, the ligand for the APJ receptor. J. Neurochem. *74*, 34–41.

Leptin, M. (2005). Gastrulation movements: the logic and the nuts and bolts. Dev. Cell *8*, 305–320.

Lin, F., Sepich, D.S., Chen, S., Topczewski, J., Yin, C., Solnica-Krezel, L., and Hamm, H. (2005). Essential roles of G{α}12/13 signaling in distinct cell behaviors driving zebrafish convergence and extension gastrulation movements. J. Cell Biol. *169*, 777–787.

Marlow, F., Zwartkruis, F., Malicki, J., Neuhauss, S.C., Abbas, L., Weaver, M., Driever, W., and Solnica-Krezel, L. (1998). Functional interactions of genes mediating convergent extension, knypek and trilobite, during the partitioning of the eye primordium in zebrafish. Dev. Biol. *203*, 382–399.

Mizumatsu, S., Monje, M.L., Morhardt, D.R., Rola, R., Palmer, T.D., and Fike, J.R. (2003). Extreme sensitivity of adult neurogenesis to low doses of X-irradiation. Cancer Res. *63*, 4021–4027.

Moorman, A.F., and Christoffels, V.M. (2003). Cardiac chamber formation: development, genes, and evolution. Physiol. Rev. *83*, 1223–1267.

Myers, D.C., Sepich, D.S., and Solnica-Krezel, L. (2002). Convergence and extension in vertebrate gastrulae: cell movements according to or in search of identity? Trends Genet. *18*, 447–455.

Nasevicius, A., and Ekker, S.C. (2000). Effective targeted gene 'knockdown' in zebrafish. Nat. Genet. *26*, 216–220.

O'Dowd, B.F., Heiber, M., Chan, A., Heng, H.H., Tsui, L.C., Kennedy, J.L., Shi, X., Petronis, A., George, S.R., and Nguyen, T. (1993). A human gene that shows identity with the gene encoding the angiotensin receptor is located on chromosome 11. Gene *136*, 355–360.

Sepich, D.S., and Solnica-Krezel, L. (2005). Analysis of cell movements in zebrafish embryos: morphometrics and measuring movement of labeled cell populations in vivo. Methods Mol. Biol. *294*, 211–233.

Sepich, D.S., Myers, D.C., Short, R., Topczewski, J., Marlow, F., and Solnica-Krezel, L. (2000). Role of the zebrafish trilobite locus in gastrulation movements of convergence and extension. Genesis *27*, 159–173.

Smit, M.J., Vischer, H.F., Bakker, R.A., Jongejan, A., Timmerman, H., Pardo, L., and Leurs, R. (2006). Pharmacogenomic and structural analysis of constitutive G protein-coupled receptor activity. Ann.u Rev. Pharmacol. Toxicol. *47*, 53–87.

Solnica-Krezel, L. (2005). Conserved patterns of cell movements during vertebrate gastrulation. Curr. Biol. *15*, R213–R228.

Solnica-Krezel, L., Schier, A.F., and Driever, W. (1994). Efficient recovery of ENU-induced mutations from the zebrafish germline. Genetics *136*, 1401–1420.

Szokodi, I., Tavi, P., Foldes, G., Voutilainen-Myllyla, S., Ilves, M., Tokola, H., Pikkarainen, S., Piuhola, J., Rysa, J., Toth, M., and Ruskoaho, H. (2002). Apelin, the novel endogenous ligand of the orphan receptor APJ, regulates cardiac contractility. Circ. Res. *91*, 434–440.

Tatemoto, K., Hosoya, M., Habata, Y., Fujii, R., Kakegawa, T., Zou, M.X., Kawamata, Y., Fukusumi, S., Hinuma, S., Kitada, C., et al. (1998). Isolation and characterization of a novel endogenous peptide ligand for the human APJ receptor. Biochem. Biophys. Res. Commun. *251*, 471–476.

Tatemoto, K., Takayama, K., Zou, M.X., Kumaki, I., Zhang, W., Kumano, K., and Fujimiya, M. (2001). The novel peptide apelin lowers blood pressure via a nitric oxide-dependent mechanism. Regul. Pept. *99*, 87–92.

Thisse, C., Thisse, B., Schilling, T.F., and Postlethwait, J.H. (1993). Structure of the zebrafish snail1 gene and its expression in wild-type, spadetail and no tail mutant embryos. Development *119*, 1203–1215.

Tucker, B., Hepperle, C., Kortschak, D., Rainbird, B., Wells, S., Oates, A.C., and Lardelli, M. (2007). Zebrafish Angiotensin II Receptor-like 1a (agtrl1a) is expressed in migrating hypoblast, vasculature, and in multiple embryonic epithelia. Gene Expr. Patterns *7*, 258–265.

Vassilatis, D.K., Hohmann, J.G., Zeng, H., Li, F., Ranchalis, J.E., Mortrud, M.T., Brown, A., Rodriguez, S.S., Weller, J.R., Wright, A.C., et al. (2003). The G protein-coupled receptor repertoires of human and mouse. Proc. Natl. Acad. Sci. USA *100*, 4903–4908.

Vicente-Manzanares, M., Webb, D.J., and Horwitz, A.R. (2005). Cell migration at a glance. J. Cell Sci. *118*, 4917–4919.

Yelon, D., and Stainier, D.Y. (1999). Patterning during organogenesis: genetic analysis of cardiac chamber formation. Semin. Cell Dev. Biol. *10*, 93–98.

Accession Numbers

Accession numbers have been deposited in the NCBI database with accession codes DQ062434 and EF079888 for Apelin and Agtrl1b, respectively.